THE JOURNAL OF PHYSICAL CHEMISTRY C

Article

pubs.acs.org/JPCC

Electron Paramagnetic Resonance Study of Copper–Ethylenediamine Complex Ion Intercalated in Bentonite

José Pedro Donoso,* Claudio J. Magon, José F. Lima, and Otaciro R. Nascimento

IFSC, Universidade de São Paulo, P.O. Box 369, 13560-970 São Carlos, São Paulo, Brasil

Eglantina Benavente

Universidad Tecnológica Metropolitana, P.O. Box 9845, Santiago, Chile

Center for the Development of Nanoscience and Nanotechnology, CEDENNA, Avda. Ecuador 3493, 9170124, Santiago, Chile

Mabel Moreno

CIC nanoGUNE Consolider, Tolosa Hiribidea 76, 20018 Donostia-San Sebastian, Spain

Center for the Development of Nanoscience and Nanotechnology, CEDENNA, Avda. Ecuador 3493, 9170124, Santiago, Chile

Guillermo Gonzalez

Facultad de Ciencias, Universidad de Chile, P.O. Box 653, Santiago, Chile

Center for the Development of Nanoscience and Nanotechnology, CEDENNA, Avda. Ecuador 3493, 9170124, Santiago, Chile

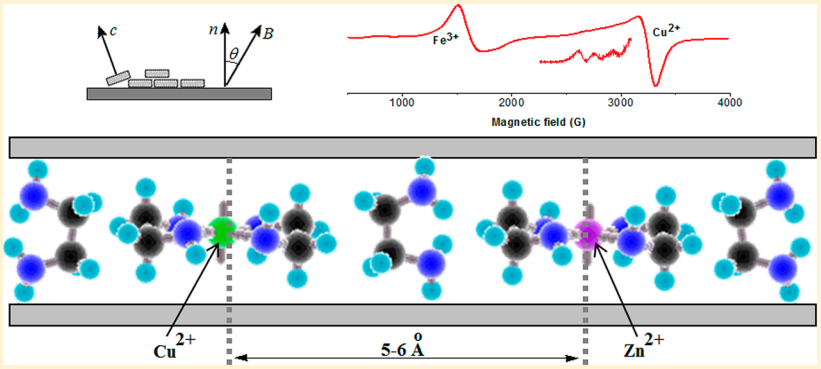

ABSTRACT: This work reports on studies of two-dimensional networks of Cu^{2+} ions, built by exchanging Na-bentonite with Cu^{2+} aqueous or with the bis(ethylenediamine) complex, $[Cu(C_2H_4(NH_2))_2]^{2+}$, at different concentrations of the paramagnetic center. Dilution of the magnetically active species is performed by the cointercalation of analogous diamagnetic zinc species, aqueous Zn^{2+}, or complexed $[Zn(C_2H_4(NH_2))_2]^{2+}$ ions, with ethylenediamine in excess. Materials were characterized by X-ray diffraction, Fourier transform infrared (FT-IR) and UV–visible spectroscopy, and continuous-wave electron paramagnetic resonance (EPR). X-ray diffraction measurements indicated that the interlaminar distance in the bentonite decreases with the increase of Zn concentration in the composites. The observation of a two-component Cu^{2+} EPR spectrum imply the coexistence of isolated Cu^{2+} with a well-resolved hyperfine structure and spin–spin exchanged Cu^{2+} dimers or clusters with an unresolved hyperfine structure. EPR spin Hamiltonian parameters of the isolated species in Cu/ethylenediamine intercalated samples are typical of axially distorted sites, six-coordinated with bis(ethylenediamine) in the equatorial plane and with oxygen on the internal surfaces of the clay. Experimental facts indicate that the interaction between paramagnetic centers is mainly favored by two different phenomena: turbostratic disorder of clay sheets and segregation of the magnetic centers leading to interstratifications of layers.

INTRODUCTION

Layered natural clays have been extensively studied in recent years because of their chemical functionality, offering a rich intercalation chemistry allowing modifying and functionalizing materials with potential technological importance.[1,2] Intercalation of guest species as metal complexes and organic molecules in the interlaminar spaces of the clay is a versatile method for the preparation of systems organized at nanoscale level

Received: August 29, 2013
Revised: October 17, 2013
Published: October 18, 2013

exhibiting new physical and chemical properties.[3−6] The intercalation properties of layered clays have found a wide variety of materials applications including chemical catalysis[7−10] and the production of clay/polymer nanocomposites.[11−13]

Bentonites are clays dominated by minerals of the smectites group, including Na and Ca montmorillonite, saponite, beidellite, and hectorite. The smectite is a layer clay mineral constituted by two silica tetrahedral sheets bonded to a central alumina octahedral sheet. Basal spacing for air-dried smectites changes from 1.26 to 1.54 nm depending on the type and valence of the exchangeable cation. Alkaline cations located in the interlaminar spaces are intrinsically exchangeable ions defining the characteristic cation-exchange capacity (CEC) of the clay.[14] On account of its higher surface area, cation-exchange capacity, retention ability, swelling capacity, low cost, and high abundance, bentonite has attracted great interest for treatment of environmental pollution. Numerous studies have been conducted on the sorption of heavy metals by bentonite,[15−20] the removal of chemical contaminants,[21−25] and the development of barrier systems for radioactive waste repositories.[26−28] Bentonites are also concerned with catalysts and catalyst supports.[29,30]

Electron paramagnetic resonance, EPR, is a sensitive spectroscopic technique for the study of local coordination of paramagnetic centers, such as Cu^{2+}, Fe^{3+}, and Mn^{2+}, in a variety of functional materials and catalytic systems.[31] Recently, a number of magnetic resonance studies have addressed the coordination of Cu^{2+} ions on clays. Early investigations used the EPR technique to examine the Fe^{3+} present in bentonotite clay and to determine the aqueous coordination and location of exchangeable Cu^{2+} cations in hydrate montmorillonite and hectorite clays.[8,32−37] Additionally, a number of studies have been focused on the coordination geometry of Cu^{2+} in copper complexes intercalated on lamellar clays.[2,38−42] With the recognition of the luminescent properties of lanthanides ions in bentonite and hectorite clay nanocomposites,[4,5,14] a more precise knowledge of the immediate environment of the paramagnetic ions in the structure, as well as the ion−ion and the ion−clay interactions, become desirable to optimize luminescent efficiency of these materials.

Given the considerable environmental importance of bentonite clay because of its potential for metal removal from contaminated water, knowledge of the local coordination of the copper ions and the structural distortions that occur upon intercalation of the copper complexes in the bentonite can help to optimize adsorbent properties of this clay. In the present work, Cu^{2+}-exchanged bentonite and Cu^{2+}-bis(ethylenediamine) complex exchanged in bentonite are investigated by EPR spectroscopy. Ethylenediamine, $C_2H_4(NH_2)_2$, designated as "en", is known to form stable complexes with a number of transition metal ions that can be intercalated into the interlayer spaces of clays.[38] To obtain a homogeneous distribution of paramagnetic ions into the two-dimensional interlayer space, the Cu^{2+} complex ions $[Cu(C_2H_4(NH_2))_2]^{2+}$ were diluted in a dense packed matrix of aqueous Zn^{2+} complex ions $[Zn(C_2H_4(NH_2))_2]^{2+}$. We also analyzed the EPR spectral contribution resulting from magnetic interactions due to spin−spin exchange coupling mechanism occurring in these natural clays. The copper ion was found to be a particularly useful probe, since it has an effective electron spin $S = 1/2$ and a nuclear spin $I = 3/2$, which allow the observation of hyperfine lines. Since Cu^{2+} EPR spectra are very sensitive to symmetry and strengths of the ligand field in the immediate environment of the paramagnetic ion, the EPR data combined with optical absorption spectroscopy can be used to obtain information about the nature of the ground state of Cu^{2+} ions, the covalency of the bonding between the copper 3d orbital and the ligand orbitals, and the presence of tetrahedral distortion around the metal in copper complexes.[40,42,43]

EXPERIMENTAL SECTION

Materials and Preparation of the Samples. Bentonite (Sigma) purified and converted in its Na^+ form used in this work is analyzed by plasma atomic absorption spectroscopy (Perkin-Elmer ICP-OES OPTIMA 1000DV) and presents the global formula $Na_{(0.47)}(Al_{1.58}Fe_{0.17}Mg_{0.25})(Al_{0.22}Si_{3.78}O_{10})$ and a characteristic ion exchange capacity (cec) value, determined experimentally,[44] of 85 mequiv/100 g. $CuCl_2$ (Merck Co), $ZnCl_2$ (Merck Co), ethylenediamine (en, Aldrich Co.), and methanol (Merck Co.) were used as received. Bidistilled water was used in the experiments which in general were performed in air.

The samples bentonite/Cu^{2+}/Zn^{2+}/H_2O were prepared by ionic exchange at room temperature. Three portions of bentonite/Na^+ of 0.4 g each were treated separately with 20 mL of mixtures of 0.1 M $ZnCl_2$ and 0.03 M $CuCl_2$ at the ratios of 1:1, 1:0.5, and 1:0.1 (v/v), respectively. The suspensions were stirred during 24 h and then sonicated for 8 h. Solid products were separated by centrifugation, washed three times with distilled water, and finally, dried at 100 °C during 24 h. Partially dehydrated samples were obtained by heating the as-prepared materials at 120 °C overnight. As displayed in Table 1, these three samples were denoted by Bt-*x*,

Table 1. Nomenclature and Stoichiometry of the Samples

sample	Zn^{2+}/Cu^{2+} initial ratio	stoichiometry of the composites exchanged in bentonite
Bt-1.0	1:1.0	$Zn(II)_{0.088}/Cu(II)_{0.082}$
Bt-0.5	1:0.5	$Zn(II)_{0.106}/Cu(II)_{0.064}$
Bt-0.1	1:0.1	$Zn(II)_{0.131}/Cu(II)_{0.039}$
enBt-1.0	1:1.0	$[Cu(en)_2]_{0.17}/(en\text{-}CO_2)_{1.2}$
enBt-0.5	1:0.5	$[Zn(en)_2]_{0.138}/[Cu(en)_2]_{0.032}/(en\text{-}CO_2)_{2.2}$
enBt-0.1	1:0.1	$[Zn(en)_2]_{0.147}/[Cu(en)_2]_{0.023}/(en\text{-}CO_2)_{1.5}$

with x = 1.0, 0.5, and 0.1 denoting the initial copper concentration relative to zinc. Stoichiometries of the samples, as determined by chemical analysis, are also displayed in Table 1. In Table 2 the chemical analysis data obtained for all prepared samples are shown.

An aqueous solution of Cu^{2+}/en complex was prepared by, initially, dissolving a 25 mM solution of copper nitrate into a 50 mM solution of en. Then, for characterization by EPR measurements, part of the mixture was dissolved in distilled water at the ratio 1:10 (v/v). The EPR spectrum measured at 50 K is shown in Figure 1A. This spectrum is characterized by a broad, asymmetric, and unstructured line centered at $g \approx 2$, typical of Cu^{2+} ions magnetically coupled, and could be well-simulated by a $S = 1/2$ spin in axial symmetry. In the first line of Table 3 the Hamiltonian parameters obtained from the simulation are presented. The observed broad line, free of hyperfine structure, occurs because the freezing and crystallization of the water segregates the Cu/en complexes into small volumes, degrading the homogeneity of the solution and promoting spin−spin exchange interactions. To maintain a homogeneous dilution of the complexes, 20% (v/v) of glycerin was dissolved into the solution, and the obtained EPR spectrum in this case is presented in Figure 1B, whose evident hyperfine interactions shows clearly the presence of two nonequivalent

dx.doi.org/10.1021/jp408658d | J. Phys. Chem. C 2013, 117, 24042−24055

Table 2. Measured and Calculated Concentrations of N, C, H, and Cu in Zn^{2+}–Cu^{2+} and $[Zn(en)]^{2+}$–$[Cu(en)]^{2+}$ Intercalated in Bentonite

	% measured (calculated)			
sample	N	C	H	Cu
Bt-1.0				1.380 (1.377)
Bt-0.5				1.080 (1.075)
Bt-0.1				0.650 (0.655)
enBt-1.0	8.21 (8.29)	10.53 (9.88)	2.63 (4.20)	2.22 (2.08)
enBt-0.5	10.19 (10.42)	13.22 (13.28)	4.34 (5.87)	0.37 (0.33)
enBt-0.1	7.97 (8.10)	10.34 (10.32)	3.49 (4.56)	0.29 (0.27)

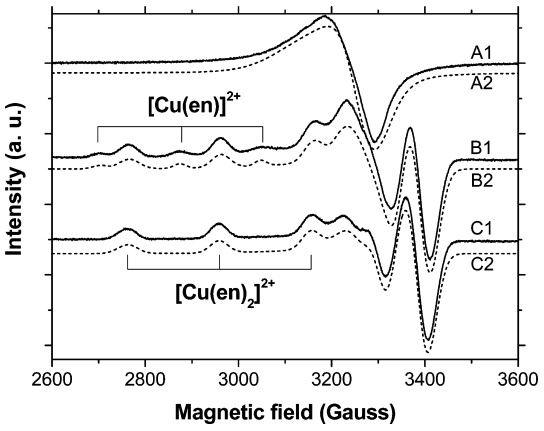

Figure 1. EPR spectra obtained at 50 K of (A) Cu/en frozen solution as prepared with ratio 1:2, (B) same sample with 20% (v/v) of dissolved glycerin, and (C) Cu/en/glycerin solution with excess of en. Numerical simulations of the spectra are plotted in dashed lines. The positions of first three lower field parallel hyperfine peaks of $[Cu(en)]^{2+}$ and $[Cu(en)_2]^{2+}$ complexes are indicated.

isolated Cu^{2+} species. As indicated by the arrows in Figure 1, this two species were assigned to the coexistence of Cu-ethylenediamine, abbreviated as $[Cu(en)]^{2+}$ and Cu-bis-(ethylenediamine), abbreviated as $[Cu(en)_2]^{2+}$, in relation 22.5:77.5%. To get a pure solution, containing only $[Cu(en)_2]^{2+}$ complexes, some amount of en in excess was added to the solution, leading to the EPR spectrum of Figure 1C, where it is evident the suppression of the less intense hyperfine peaks associated to the $[Cu(en)]^{2+}$ complex. This last solution, before dissolution of glycerin, had a pH value of 6.5 and was used for the UV–vis absorption spectrum measurement to be presented ahead. The spin Hamiltonian parameters obtained from the simulations (Table 3) are consistent with those previously reported in the literature for $[Cu(en)_2]^{2+}$, $g_{\|} = 2.21$, $g_{\perp} = 2.05$, and $A_{\|} = 600$ MHz (200×10^{-4} cm^{-1}),[38,45−47] and for $[Cu(en)]^{2+}$, $g_{\|} = 2.26$, $g_{\perp} = 2.05$, and $A_{\|} = 540$ MHz (180×10^{-4} cm^{-1}).[38,46]

Samples of bentonite/$[Zn(en)_2]^{2+}$/$[Cu(en)_2]^{2+}$/en were obtained by treating separately three clay portions of 0.4 g each with 20 mL of mixtures 1:1, 1:0.5, and 1:0.1 (v/v) of 0.1 M $[Zn(en)]Cl_2$ and 0.03 M $[Cu(en)_2]Cl_2$ respectively. The suspensions were stirred during 24 h and sonicated for 8 h. The solids separated by centrifugation were treated three times with pure ethylenediamine, then washed twice with methanol to eliminate excess of amine, and dried at 60 °C for 24 h. Labeling of the obtained samples is referred along this article to the volume ratio in the solution mixtures used for the intercalation and abbreviated as enBt-*x*, with $x = 1.0$, 0.5, and 0.1 (see Table 1).

To prepare partially oriented films, 4 mg of sample enBt-0.5 was stirred in 4 mL of bidistilled water and sonicated for 1 h. Then, about 1/4 of the volume was drop-cast on 10 thin glass plates, with surface of 3 mm × 20 mm each, and dried at 40 °C for 1 h. The homogeneity of grain distribution on the dried plates was checked under an optical microscope. The procedure was repeated four times, by recasting the remainder parts of the solution on the previously dried plates. Finally, the 10 plates were stacked up in a single package. The obtained product will be referred to by the abbreviation enBt-0.5-film. Using chemical analysis data (Table 2), the estimated number of copper ions in the whole package was about 10^{15}–10^{16}, a reasonable amount for standard continuous wave EPR measurements.

Chemical Characterization of the Samples. The composition of the samples was determined by combustion analysis (C, H, N, SISONS ES-1108) and by atomic absorption (Cu, Zn, spectrometer Perkin-Elmer 3100). The composition and structure of the samples were analyzed by powder X-ray diffraction analysis (DRX, Siemens D-5000, Cu K radiation), FT-IR (Bruker Vector 22), and UV–visible absorption and reflectance spectroscopy (Shimadzu 2450).

Electron Paramagnetic Resonance. Continuous-wave (CW) EPR spectra were obtained in the temperature range of 4 K to room temperature on a Bruker Elexsys E580 spectrometer operating at the X-band (≈ 9.5 GHz). The temperature was controlled by a continuous flow liquid helium Oxford cryogenic system, model ITC503. In case of powder samples, a small amount of the material was inserted in the bottom of a 3 mm inner diameter quartz tube. In case of the package of film plates, they were accommodated at the bottom of a 4 mm inner diameter quartz tube inside a goniometer, such that the static magnetic field direction could rotate in a plane perpendicular to the longest dimension of the plates. Solid state powder EPR

Table 3. EPR Parameters of Cu^{2+}/en Solutions[a]

spectrum	assignment	$g_{\perp}$	$g_{\|}$	$A_{\perp}$ (MHz)	$A_{\|}$ (MHz)	weight (%)	frequency (GHz)
Figure 1A	clusters	2.074	2.160				9.4751
Figure 1B	$[Cu(en)]^{2+}$	2.058	2.280	45.2	541.0	22.5	9.4498
	$[Cu(en)_2]^{2+}$	2.044	2.205	64.8	598.6	77.5	
Figure 1C	$[Cu(en)_2]^{2+}$	2.043	2.206	74.0	595.0		9.4388

[a]Line broadening parameters are not shown. The nomenclature is defined in the Results and Discussion section.

dx.doi.org/10.1021/jp408658d | J. Phys. Chem. C 2013, 117, 24042−24055

spectra were simulated by the well-known software package named EasySpin,[48] implemented in MATLAB (MathWorks, Inc.).

RESULTS AND DISCUSSION

The influence of the magnetic couplings in the EPR spectra is a common and well-known problem[31] and is particularly evident in the case of copper ions in highly concentrated samples. This effect is enhanced in the case of montmorillonite clays, where paramagnetic ionic species are confined in a two-dimensional space with fixed volume and ionic strength, both determined by the characteristic ion exchange capacity (cec) of the clay. Moreover, because of the intrinsic microheterogeneity of the layered structures, the intercalated ions are immersed in a mobile, liquid-like phase, defined by relatively weak interactions between the cations and the rigid surface of the polyanionic aluminosilicate sheets. Our approach, to simultaneously optimize the concentration, distribution, and immobility of ionic copper species intercalated in bentonite, was the cointercalation of an analogous Zn^{2+} species, which are expected to have a guest behavior similar to that of Cu^{2+}. Although Cu^{2+} and Zn^{2+} have similar ionic radii (0.72 Å and 0.74 Å, respectively), Cu^{2+} is more sensitive to ligand field interactions, which may produce some additional structural and thermodynamic effects. Because of charge effects, the exchange of Na^+ ions in the bentonite, used as starting material, by divalent cations like aqueous Zn^{2+} and Cu^{2+} ions or their corresponding complexes with ethylenediamine, is always a thermodynamically favorable and a relatively fast process. In both cases, the formation of ethylenediamine complexes in situ is also straightforward due to their stability.

In Table 1 are reported the stoichiometries of the intercalates prepared by using aqueous solution mixtures of the respective cationic species at different Zn^{2+}/Cu^{2+} and $[Zn(en)_2]^{2+}/[Cu(en)_2]^{2+}$ ratios. Due to the tendency of amines inserted in inorganic matrices to absorb atmospheric water and carbon dioxide,[49] some deviations between calculated and experimental analyses are observed. As shown in Table 2, experimental analyses fit relatively well with calculated values global formulas considering the absorption of 1 mole of CO_2 per moles of amine. Notwithstanding, calculated stoichiometries, particularly the metal/amine ratios, are reproducible within a small range and certainly enough for understanding the nature of the obtained nanocomposites. In all cases, the amount of intercalated divalent cations agrees with the cec of the clay. However, the affinity of the bentonite for Cu^{2+} appears to be higher than that for Zn^{2+}. This difference is much more notorious in the case of the complexes. For instance, the sample obtained from divalent cation mixtures 1:1 (v/v), that is, with a Zn^{2+}/Cu^{2+} molar ratio of about 3.3:1, solely contains copper ions as the intercalated species. Analytical results also show that the nanocomposites contain an excess of amine, that is, more than three en-molecules per metal atom.

Despite the similarity of the molecular structure dimensions of both zinc/and copper/en complexes, they present some slightly structural differences in the intercalated state. In Figure 2 the X-ray diffraction patterns of bentonite/Na^+ as well as samples enBt-x for x = 1.0, 0.5, and 0.1 are reproduced. All species show the characteristic Bragg reflection 001 corresponding to their respective interlaminar distances. An interplanar repeating distance, of approximately 9.96 Å in the precursor bentonite/Na^+, clearly increases with the intercalation of ethylenediamine metal complexes. Sample enBt-1.0, containing no zinc, shows an interlaminar distance of 13.7 Å,

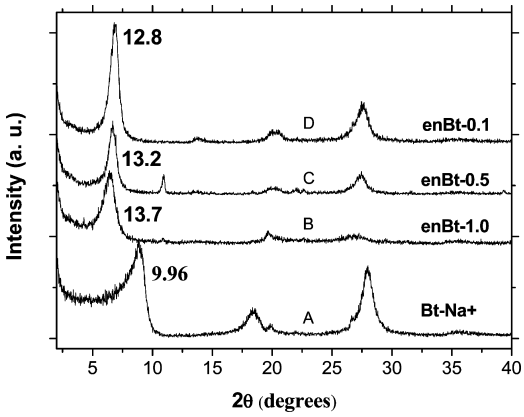

Figure 2. X-ray diffraction patterns of pure bentonite-Na^+ (A) and samples enBt-x, with x = 1.0 (B), 0.5 (C), and 0.1 (D). The interlaminar distances, in Å, determined from the characteristic Bragg reflection 001, are indicated beside each corresponding peak.

which slightly decreases with increasing amount of zinc complex in the sample.

To get information on the nature of intercalated copper/zinc complexes, samples enBt-0.5 and enBt-1.0 were, respectively, analyzed by vibrational (IR) and electronic (UV–vis) spectroscopy. In Figure 3 the FT-IR spectrum is shown in the range

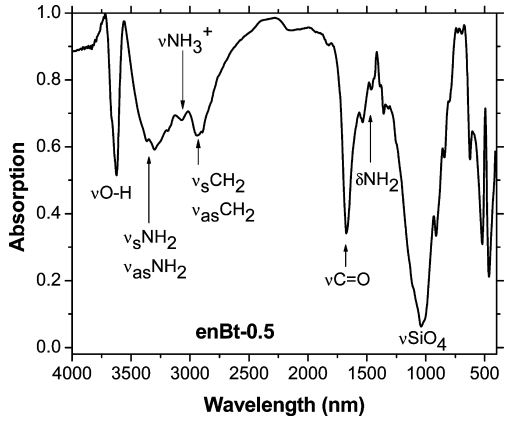

Figure 3. IR absorption spectrum of sample enBt-0.5.

4000–500 cm^{-1}, where the presence of ethylenediamine coordinated with metal ions may be detected by the presence of absorption bands at 3260 and 3280 cm^{-1} attributed to $-NH_2$ symmetric and asymmetric stretching, respectively, as well as at 2920 and 2950 cm^{-1} assigned to $-CH_2$ symmetric and asymmetric stretching frequencies.

Information upon the configuration of the first coordination sphere in the intercalated complex can be obtained from the UV–visible reflectance spectrum illustrated in Figure 4 (solid line). The reflectance maximum at 514 nm (19455 cm^{-1}) corresponds to a complex ion with one or two ethylenediamine molecules per Cu atom, but not to $[Cu(en)_3]^{2+}$, for which an absorption maximum at 16408 cm^{-1} has been reported.[38] Given the relative stability of ethylenediamine/copper complexes and the procedure used for the preparation of the composites, it is reasonable to hypothesize the formation of $[Cu(en)_2]^{2+}$ in clay interlaminar space. For reference, the UV–visible absorption spectrum of aqueous solution of $[Cu(en)_2]^{2+}$ complex was also acquired (dashed line) and shows an

dx.doi.org/10.1021/jp408658d | J. Phys. Chem. C 2013, 117, 24042–24055

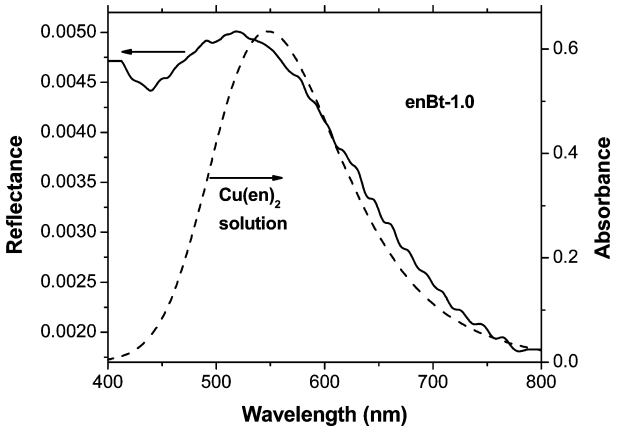

Figure 4. UV−visible absorption spectrum of $Cu(en)_2$ complex in solution (dashed line) and reflectance spectrum of sample enBt-1.0 (solid line).

absorption maximum at 548 nm (18248 cm^{-1}), in agreement to the value 18315 cm^{-1} reported earlier.[45]

As commented above, the amine contained in the products exceeds the stoichiometry of $[Cu(en)_2]^{2+}$, so the presence of additional ligand has to be assumed. The cointercalation of the free ligand may be understood by considering the fraction of sheet surface area involved in the interaction with the metal complex. Indeed, considering that the cec of the bentonite (83 mequiv/100 g) corresponds to about 0.5 equiv per Si_4 unit, there is much room, at least 50% of the sheet surface area, which could host the free excess of ligand. Intercalation of additional species was also observed in organoclays with stoichiometries exceeding by far the cec of the clay.[50] Therefore, the saturation of the interlaminar space with additional amine-derivate is attained.

The structure of the intercalated interlaminar space may be furthermore studied by contrasting available experimental structural and composition data, through molecular modeling using van der Waals atomic radii, taking into account both the surface available on clay laminas and the volume described by the metal complexes and free ligand performed above. Molecular models of guest species possibly intercalated in bentonite, namely, $[Cu(en)_3]^{2+}$, $[Cu(en)_2]^{2+}$, and $[Zn(en)_2]^{2+}$ and ethylenediamine, were analyzed and considered for building the scheme proposed in Figure 5. The comparison of the dimensions of $[Cu(en)_3]^{2+}$ ion with the experimental interlayer distance definitively discards its presence in the final products. It is interesting to remark the incorporation of only two ethylenediamine molecules into its first coordination sphere in spite of the great excess of ligand which, in the case of the free complex, would easily lead to the formation of $[Cu(en)_3]^{2+}$. This indicates that the confinement effect produced by the clay is saturating the axial five and six coordinations positions of the complexes, as further discussed below.

Some facts can be extracted from the available stoichiometry of the products and the structure proposed in Figure 5. First, one must consider that about 0.17 mol of copper complex per Si_4 unit can occupy 8.33 A^2 if free rotation around the complex C2 principal axis is hypothesized. Second, since the metal complexes occupy about 31% of the clay surface area, which is about 27 A^2 per Si_4 unit, the remaining area is enough for inserting of additional free ligands. Therefore, saturation of the available space by insertion of about 2 mol of en per Si_4 unit, as deduced from our experiments, is a reasonable assumption. From these results we can conclude that the minimum copper−copper distance in the enBt-1.0 sample is in the range 5−6 Å and, moreover, that these centers are fixed in a matrix in which practically all low energy sites are saturated, thus making difficult eventual exchange processes. This approach, which to the best of our knowledge has not been used before in two-dimensional microheterogeneous systems, produces results especially useful for performing EPR studies like those described below.

EPR Spectra of Cu^{2+} Exchanged-Bentonite. Figure 6 shows the X-band CW-EPR spectra measured at 4 K of the

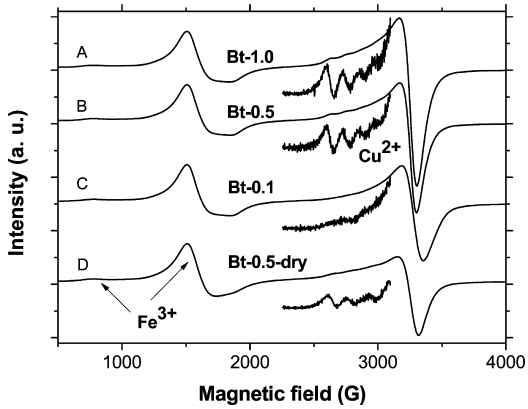

Figure 6. X-band EPR spectra measured at 4 K of the samples Bt-1.0 (A), Bt-0.5 (B), Bt-0.1 (C), and Bt-0.5 after a overnight dehydration at 120 °C (D). Resonance bands associated to Fe^{3+} and Cu^{2+} ions are indicated. Signal intensities are normalized to the Fe^{3+} resonance band. The noisier segments correspond to the derivative of the EPR spectra around the $g_{\|}$ region.

Cu^{2+} in samples Bt-*x*. Two prominent features with effective *g*-values $g \approx 4.3$ and $g \approx 2.0$ appeared in all spectra. The former signal, which has been frequently reported in montmorillonite clays[8,51,52] and in glasses,[53−55] is attributed to isolated Fe^{3+} ions in tetrahedral or octahedral symmetry with rhombic distortion. The Fe^{3+} ion has a $3d^5$ electronic configuration, spin $S = 5/2$, and ground state $^6S_{5/2}$. When this S-state ion is introduced in a solid structure, the energy levels are affected by the crystal field produced by the neighboring ions. The EPR spectra of Fe^{3+} ions can be well-described in terms of the spin Hamiltonian:[31]

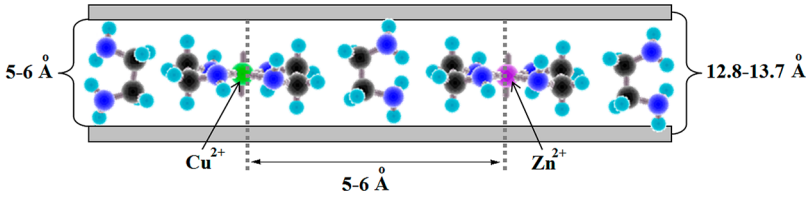

Figure 5. Schematic representation of bentonite−$[Cu(en)_2]$−$[Zn(en)_2]$−en complexes (green: copper, purple: zinc, black: carbon, dark blue: nitrogen, light blue: hydrogen).

dx.doi.org/10.1021/jp408658d | J. Phys. Chem. C 2013, 117, 24042−24055

$$H = \beta HgS + D\left[S_z^2 - \frac{1}{3}S(S+1)\right] + E(S_x^2 + S_y^2) \quad (1)$$

H is the applied magnetic field; S_x, S_y, and S_z are components of spin along three mutually perpendicular crystalline axes x, y, and z; D and E are the second-order crystal field terms with axial and rhombic symmetry, respectively.

In the limiting case $|E/D| = 1/3$, the $g = 4.3$ resonance of Fe^{3+} ions, as arising from the middle doublet among three Kramer's doublets, $|\pm 1/2\rangle$, $|\pm 3/2\rangle$, and $|\pm 5/2\rangle$, is typical of fully rhombic symmetry.[31,56] Therefore, the observed signal at $g = 4.3$ in our bentonite clays can be attributed to isolated Fe^{3+} impurities in octahedral or tetrahedral symmetry with rhombic distortion, in coordination sites of the clay structure.[8,57] Because of the similarity of the Fe^{3+} and Al^{3+} ionic radii (R(Fe) = 0.65 Å, R(Al) = 0.53 Å) and the equality in their charges, Fe^{3+} is expected to substitute Al^{3+} ions in the interior of the clay sheets.

The high field part of the EPR spectra in Figure 6 (above 2500 G) is attributed to Cu^{2+} ions in the interlayer space of samples Bt-x. A closer examination of these spectra demonstrate that the intense line around 3300 G cannot be explained by taking into account only isolated Cu^{2+} species. This fact is evident in the case of sample Bt-0.1, which shows no trace of the hyperfine parallel peaks. Therefore, the spectra of samples Bt-x must be assigned to, at least, two different Cu^{2+} species: isolated single spin and magnetically coupled pairs or clusters, hereafter designated by Cu-A and Cu-B, respectively. Essentially, we are suggesting that the spectra in Figure 6 are composed by components Cu-A, characterized by a hyperfine structure arising from isolated Cu^{2+} ions and Cu-B, a broad and more intense resonance line free of hyperfine peaks, which is attributed to Cu^{2+} ions coupled by spin−spin exchange interactions.

The isolated copper spectra indicate dilute Cu^{2+} species in axially distorted sites coordinated with hydroxyl groups and water molecules in the interlayer space and with the surface oxygen of the alumino-silicate sheets along the c-axis of the bentonite clay. Since the Cu^{2+} ion has a $3d^9$ electronic configuration, electronic spin $S = 1/2$ and the nuclear spin for the ^{63}Cu and ^{65}Cu isotopes (natural abundance 69.1% and 30.9%, respectively) is $I = 3/2$, and the EPR spectrum of the Cu^{2+}/Zn^{2+}/bentonite consists of a set of four perpendicular and four parallel hyperfine components. This hyperfine structure results from the dipole−dipole interaction between the magnetic moment of the ^{65}Cu and ^{63}Cu nuclei and the electronic moment of the unpaired Cu^{2+} electrons. The low field part of the copper spectra in Figure 6 (around 2800 G), corresponding to $g_{\|}$, shows a set of four broad hyperfine lines barely identified in the acquired spectra but, apparent in the second derivative of the absorption signal, plotted in Figure 6 just around the $g_{\|}$ region. It is noted that the copper hyperfine structure is clearly visible for the more concentrated samples Bt-1.0 and Bt-0.5, while invisible for the less concentrated sample Bt-0.1. In the high field part of the spectra (≈ 3200 G), corresponding to $g_{\perp}$, the copper hyperfine satellites are not resolved, leading to an intense single line in this field region.

The Cu^{2+} EPR spectrum of isolated sites (Cu-A) is described by an axial spin Hamiltonian, which includes both Zeeman and hyperfine interactions,

$$H = g_{\|}\beta H_z S_z + g_{\perp}\beta(H_x S_x + H_y S_y) + A_{\|} I_z S_z + A_{\perp}(I_x S_x + I_y S_y) \quad (2)$$

Here, z is the axial symmetry axis; β is the Bohr magneton; H_x, H_y, and H_z are the components of the applied magnetic field; S and I are the electron and the nuclear spin operators; $g_{\|}$ and $g_{\perp}$ are the parallel and perpendicular components of the anisotropic tensor g, and $A_{\|}$ and $A_{\perp}$ are the parallel and perpendicular hyperfine components of the hyperfine tensor A. The first two terms in eq 2 represent the interaction between the electronic spin and the magnetic field and the third and fourth terms the hyperfine coupling between electronic and nuclear spins.

To create a scenario that fully explains the lineshapes of the spectra in Figure 6, we propose that the origin of the broad component has a simple explanation based on the Anderson theory for narrowing of spectral lines by electronic spin−spin exchange interactions,[58] which was later extended to hyperfine lines for nuclear spins greater than 1/2.[59] To account for the physical mechanism we hypothesize that the Cu^{2+} complexes can be coupled between themselves by weak exchange interactions that can be promoted by hydrogen bridges. The main parameters involved in the theory are the hyperfine coupling constant A and the strength of the exchange interaction J. In the absence of exchange ($J = 0$) the hyperfine structure arising from a nuclear spin $I = 3/2$ consists of four equally spaced hyperfine lines having almost the same amplitude and width. When J becomes comparable to A, the exchange may produce broadening, narrowing, or a total collapse of the hyperfine structure into a single line, depending on the strength of the interaction. This phenomenon has been observed in many other copper compounds; for instance, in single crystals of copper-amino acid salts.[60] Based on this theory, we believe that the broad, intense, and unstructured line observed in the spectra of Figure 6 is due to a weak spin−spin exchange interaction between paramagnetic centers, possibly Cu^{2+} dimers, of the order of $J \approx A_{\|} \approx 400$ MHz (≈ 20 mK).

Based on the above hypothesis, the EPR spectra of Figure 6 can be interpreted and successfully simulated considering only two main contributions. First, the isolated and axially coordinated Cu^{2+} complexes (Cu-A) that do not experience any kind of interactions with neighboring paramagnetic centers, for which, the appropriated spin Hamiltonian is that of eq 2, are taken into account. Second, the Cu^{2+} complexes (Cu-B) that are close enough to each other and experience a small exchange interaction, of the order of 20 mK, are considered. For this second contribution, the same spin Hamiltonian of eq 2 is used, with the last two terms corresponding to the hyperfine interaction being neglected. In essence, this procedure is equivalent to take, for the Cu-B contribution, isolated Cu^{2+} complexes subject only to the axial Zeeman interaction.

Numerical simulation of the spectra of Figure 6 was performed on the second derivative of the absorption signal, and the results are shown in Figure 7 and Table 4. In the case of sample Bt-0.1 the hyperfine lines are not visible; therefore, its spectrum was simulated considering only species Cu-B. The estimated parallel spin Hamiltonian parameters of Cu-A species in samples Bt-1.0 and Bt-0.5 are close to $g_{\|} = 2.404$ and $A_{\|} = 410$ MHz (137×10^{-4} cm^{-1}) for both spectra. These values are consistent with those previously reported in the literature for Cu^{2+} exchanged montmorillonite, kaolinite, and laponite clays.[32,40,61] The fractional spectral intensity of species Cu-A is about 30% for both samples, Bt-1.0 and Bt-0.5, as estimated from the "Area" data in Table 4.

Plots in Figure 6B and D and corresponding simulations in Figure 7B and D show the EPR spectra of the sample Bt-0.5 before and after an overnight dehydration at 120 °C,

dx.doi.org/10.1021/jp408658d | J. Phys. Chem. C 2013, 117, 24042−24055

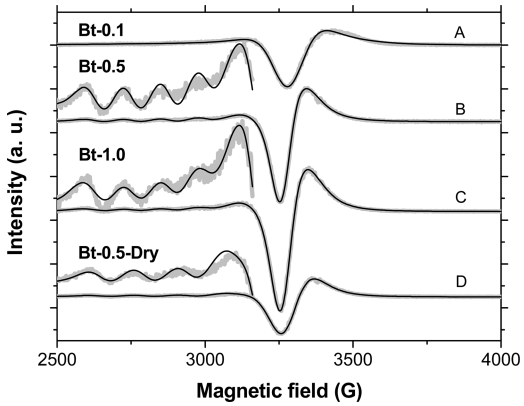

Figure 7. Numerical simulation of the Cu^{2+} X-band second derivative EPR spectra measured at 4 K for the BtCu-*x* samples. Experimental spectra are shown in thick gray traces and the fitting in solid black lines. For better visualization, the parallel segments of spectra B–D magnified 10 times are also shown. Signal intensities are normalized to the Fe^{3+} resonance band.

respectively. According to the thermogravimetric analysis (TGA), the free water can be removed from natural bentonite by thermal treatment at 120 °C.[52] The analysis of the Cu-A spectra in Figure 6D and 7D yield $g_{\|}$ = 2.360 and $A_{\|}$ = 480 MHz (160 × 10^{-4} cm^{-1}), with a decrease in the fractional spectral intensity to about 25% (see Table 4). Similar changes in the axial parameters ($g_{\|}$ and $A_{\|}$) were observed in hydrated Cu^{2+} and Mg^{2+} exchanged montmorillonite,[32] where the $A_{\|}$ coupling constant increased significantly, from 145 × 10^{-4} cm^{-1} for the hydrated sample to 172 × 10^{-4} cm^{-1} for the partially dehydrated one, with small changes in *g*-values. Also, after complete dehydration of the clay by evacuation at 150 °C, they observed that the $A_{\|}$ coupling decreases to 115 × 10^{-4} cm^{-1}. These changes were ascribed to the different Cu^{2+} species, identified as a function of the hydration level: $Cu(H_2O)_6^{2+}$ in a distorted octahedral symmetry for the fully hydrated sample, Cu^{2+} in square-planar coordination for the partially dehydrated one and Cu^{2+} inside cavities for the complete dehydrated clay.[32] Similar trends of the axial parameters with the hydration level were observed in Cu^{2+}-exchanged gallosilicate[62] and Cu^{2+}-exchanged mesoporous aluminosilicate.[63]

The change of the $A_{\|}$ coupling constant observed in our Cu^{2+} exchanged-bentonite, from 137 × 10^{-4} cm^{-1} of the original sample to 160 × 10^{-4} cm^{-1} of the dehydrated one, shows that this parameter is particularly sensitive to the local environment modifications of the cupric ion during the drying process. The spin Hamiltonian parameters of the dried sample suggest that the bentonite still retains the sorbed water after the dehydration at 120 °C.

An interesting fact regarding the copper spectra in Figure 6 is that the higher concentrated samples are the ones presenting the most intense Cu-A contribution, as can be concluded from their higher relative intensity between hyperfine structured spectrum and broad line (Table 4). In contrast, the Cu-A spectrum of the less concentrated sample, Bt-0.1, shows no evident traces of isolated Cu^{2+} species and can be assigned almost exclusively to copper pairs or clusters. In summary, EPR results on aqueous Cu^{2+}/Zn^{2+} exchanged bentonite samples support the view that the paramagnetic copper centers are not uniformly distributed in the interlaminar space of the clay, at any concentration, suggesting a tendency to clustering that increases as the concentration of copper decreases.

In view of these findings, the present work has proposed a sample preparation procedure that simultaneously optimizes the concentration, distribution, and immobility of ionic copper species intercalated in bentonite. The following sections will show and discuss the results obtained by the proposed preparation method.

EPR Spectra of $[Cu(en)_2]^{2+}$ Exchanged-Bentonite. The EPR spectra of the samples enBt-*x* are presented in Figure 8.

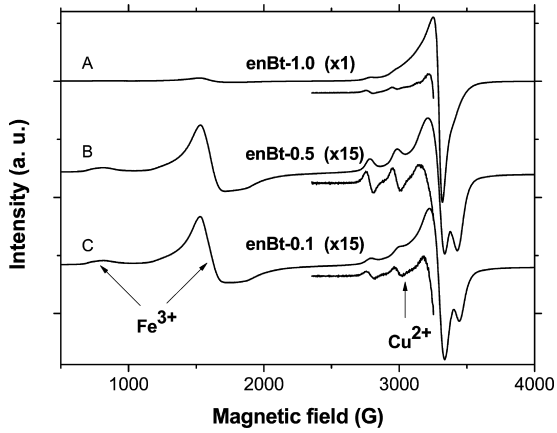

Figure 8. X-band EPR spectra measured at 4 K of the samples enBt-1.0 (A), enBt-0.5 (B), and enBt-0.1 (C). Resonance bands associated to Fe^{3+} and Cu^{2+} ions are indicated. Signal intensities are normalized to the Fe^{3+} resonance band. For a better visualization, spectra B and C are magnified 15 times. The noisier segments correspond to the derivative of the EPR spectra around the $g_{\|}$ region.

At the high field region, above 2500 G, the well-resolved hyperfine structure visible in both parallel and perpendicular

Table 4. Spin Hamiltonian Parameters for the Spectra of Figure 7[a]

	sample	area[b]	$g_{\perp}$	$g_{\|}$	$A_{\perp}$ (MHz)	$A_{\|}$ (MHz)	lwpp[c] (G)	$Hs_{\perp}$[d] (MHz)	$Hs_{\|}$[d] (MHz)
Cu-A	Bt-0.1								
	Bt-0.5	2.44	2.088	2.404	8.25	413	27.4	400	260
	Bt-0.5-Dry	1.40	2.085	2.360	6.5	480	40	388	264
	Bt-1.0	3.43	2.085	2.403	10.3	410	20.7	432	350
Cu-B	Bt-0.1	7.96	2.063	2.280			67	276	2160
	Bt-0.5	5.39	2.079	2.360			57	128	1831
	Bt-0.5-Dry	4.10	2.071	2.358			74	202	1486
	Bt-1.0	6.85	2.078	2.361			57	141	1822

[a]Notation Cu-A and Cu-B designate the two simulated components; isolated and coupled spins, respectively. [b]Area corresponds to the value of the integral of the absorption line. [c]lwpp stands for the Lorentzian line width for isotropic magnetic-field domain broadening (peak-to-peak, in G). [d]Hs is the Gaussian residual line width (full width at half height, in MHz), describing broadening due to unresolved hyperfine couplings.

dx.doi.org/10.1021/jp408658d | J. Phys. Chem. C 2013, 117, 24042–24055

regions, imply unequivocally in the existence of isolated Cu^{2+} species, coordinated in axially distorted octahedral complexes that can be satisfactorily described by the spin Hamiltonian presented in eq 2. However, as in the case of the spectra of samples Bt-*x* described in the last section, the anisotropic EPR spectra of Figure 8 must also be assigned to, at least, two different Cu^{2+} species: isolated single spin complexes (less intense structured spectrum) and magnetically coupled pairs or clusters (more intense and broad spectrum). The first copper species will be referred to as enCu-A and the second by enCu-B. To account for the physical mechanism we hypothesize that the $[Cu(en)_2]^{2+}$ complexes can be coupled between themselves by weak exchange interactions that can be promoted by the organic molecules and hydrogen bridges.

The deconvolution of the EPR spectra of Figure 8 in two components is the first step toward the understanding of the physics involved in the intercalation process of the Cu/en complexes. The hyperfine structured spectrum can give information about the local coordination of Cu^{2+} species, while the broad component can be used as a monitor for analyzing long-range structural and magnetic properties of the intercalated.

Based on the above hypothesis, the EPR spectra of samples enBt-*x* displayed in the Figure 8 were simulated, and the results are shown in Figure 9 and Table 5. In this figure it is shown

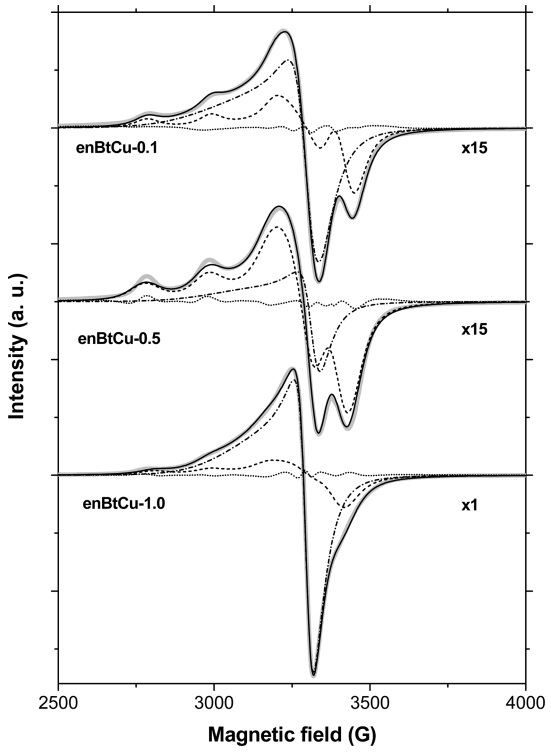

Figure 9. Numerical simulation of the Cu^{2+} X-band EPR spectra measured at 4 K for the enBtCu samples. Experimental spectra are shown in thick gray traces and the fitting in solid black lines. All spectra are composed by two components: isolated species (dashed lines) and magnetically coupled species (dash−dot−dashed lines). The fitting residue is also shown (dotted lines).

separately each one of the two spectral components used in the simulation, associated to enCu-A and enCu-B species. The quality of the fittings can be appreciated by examination of the residue that is calculated from the subtraction of the experimental data and the corresponding fitted spectra. The simulation parameters used for the fitting are displayed in Table 5.

Detailed quantitative information on the coordination environment of Cu^{2+} ions in the $Cu(en)_2$ exchanged-bentonite can be obtained by analyzing the EPR spin Hamiltonian parameters presented in Table 5. The fact that $g_{\parallel} > g_{\perp} > g_e$ (g_e = 2.0023) suggests that the ground state for the paramagnetic electrons is the d_{x2-y2} orbital ($^2B_{1g}$ state) with the Cu^{2+} ions being located in distorted octahedral sites elongated along the *z*-axis. As mentioned above, the $g_{\parallel}$ and $A_{\parallel}$ values suggest the presence of a tetra-coordinated $[Cu(en)_2]^{2+}$ complex in a square planar environment with the Cu^{2+} ion coordinated with nitrogen in the equatorial plane and with at least one oxygen in the *z*-axis.

The parallel components, $g_{\parallel}$ and $A_{\parallel}$, are sensitive to changes in geometry and ligand binding and, therefore, can be used to interpret experimental EPR data. The empirical model originally suggested by Blumberg and Peisach correlates the Cu^{2+} pair of parameters ($g_{\parallel}$ and $A_{\parallel}$) and has been applied extensively to proteins and copper-exchanged zeolites.[31,64,65] When the EPR parameters are plotted in a $g_{\parallel}$ versus $A_{\parallel}$ graph, a correlation can be found between these values and the nature of the equatorial coordinating atoms. As expected, the $g_{\parallel}$ and $A_{\parallel}$ parameters of the Bt-*x* samples fall within the specific region corresponding to the coordination of Cu^{2+} ions only by oxygen, whereas those of the Cu/en solution and enBt-*x* samples fall in the region corresponding to copper ions coordinated with nitrogen atoms and oxygen atoms.[31,65]

Regarding the spin Hamiltonian parameters for the enBt-*x* samples (Table 5) it is important to observe that the calculated $g_{\parallel}$ and $A_{\parallel}$ parameters indicate no accentuated distortion of the $[Cu(en)]^{2+}$ complex geometry when intercalated in the lamellar bentonite clay, if compared to the free complex in solution (Table 3). The empirical factor $f = g_{\parallel}/A_{\parallel}$ (cm), which is a measure of the tetrahedral distortion around the metal in tetragonally coordinated copper complexes,[42,66] can be calculated for our enBt-*x* samples, by using the spin Hamiltonian parameters in Table 4. The *f*-values of our samples are 107, 108, and 121 cm for *x* = 0.1, 0.5, and 1.0, respectively, within the range 105−135 cm assigned for tetragonal structures.[66] A comparison of the *f* values of our $Cu(en)_2$ exchanged bentonite samples with that calculated for $Cu(pyalen)^{2+}$ immobilized in laponite clay (f = 108),[42] $Cu(cyclam)^{2+}$ intercalated in hectorite and saponite clays (f = 109),[41] Cu(TMPyP) porphyrin in Na hectorite (f = 108)[2], and Cu(bis-oxazoline) immobilized in laponite (f = 132)[40] also indicate that these copper complexes does not undergo a significant distortion when intercalated in these lamellar clays.

To discuss the nature of the copper ligand bonding in terms of the magnetic parameters, the bonding coefficients can be calculated by the molecular orbital theory approach.[31,67,68] According to this approach, the nature of the bonding are described in terms of the covalency parameters α^2 and β^2. The first one, α^2, describes the covalency of the in-plane σ-bonding between a copper 3d orbital and ligand orbitals, quantifying the delocalized electronic density on the ligand atoms. Its value decreases with increasing covalency to a minimum value of α^2 = 0.5 for a completely covalent copper−ligand bond, up to a maximum value of α^2 = 1.0 for a completely ionic bond. It should be noted that within the framework of the MO model approach, because the overlapping integral between the *d* orbital of the copper ion and the *p* orbital of the ligand atoms is

dx.doi.org/10.1021/jp408658d | J. Phys. Chem. C 2013, 117, 24042−24055

Table 5. Spin Hamiltonian Parameters for the Simulated Spectra of Figure 9[a]

	sample	area	$g_\perp$	$g_\parallel$	$A_\perp$ (MHz)	$A_\parallel$ (MHz)	lwpp (G)	$Hs_\perp$ (MHz)	$Hs_\parallel$ (MHz)
enCu-A	enBt-0.1	0.4	2.039	2.190	92	615	44	167	101
	enBt-0.5	0.87	2.057	2.198	50	611	46	193	182
	enBt-1.0	3.45	2.043	2.201	72	546	61	164	103
enCu-B	enBt-0.1	0.55	2.053	2.206			46	137	1036
	enBt-0.5	0.21	2.044	2.203			43	56	873
	enBt-1.0	6.79	2.056	2.175			37	35	832

[a]Notation enCu-A and enCu-B designate the two simulated components: isolated and coupled spins, respectively. The remaining nomenclature is the same as that of Table 4.

not negligible, it is not feasible to indicate precisely the nature of the bonds but only provide trends. The covalency parameter α^2 can be evaluated from the EPR spin Hamiltonian parameters by using the simplified expression[31,67,69]

$$\alpha^2 = \frac{A_\parallel}{P} + (g_\parallel - 2) + \frac{3}{7}(g_\perp - 2) + 0.04 \quad (3)$$

where $P = 0.036\ cm^{-1}$ is the dipolar hyperfine coupling constant for free Cu^{2+}. The coefficient β^2 describes the covalency of the in-plane π-bonding. The smaller the value of β^2, the greater the covalent nature of the bond. To evaluate the parameter β^2 the EPR and UV−vis spectral data are correlated,[45]

$$g_\parallel = g_e\left[1 - \frac{4\lambda\alpha^2\beta^2}{\Delta E_{xy}}\right] \quad (4)$$

where ΔE_{xy} is the energy corresponding to the transition $^2B_{1g} \rightarrow {}^2B_{2g}$ and λ is the spin−orbit coupling constant ($\lambda = -828\ cm^{-1}$ for Cu^{2+}). Here, ΔE_{xy} was assumed to be the peak energy of the only one absorption observed in the 500−600 nm region of the UV−vis spectra (Figure 4). Using eqs 3 and 4, the bond coefficients α^2 and β^2 were evaluated for the Cu/en solution ($\alpha^2 = 0.81$, $\beta^2 = 0.70$) and for the enBt-0.1 and enBt-0.5 samples ($\alpha^2 = 0.77$ and 0.83, $\beta^2 = 0.70$). The values of α^2 obtained for the Cu/en solution ($\alpha^2 = 0.81$) are consistent to those reported earlier.[45] The covalent nature of bonding between metal and ligand orbital emerge from the fact that the bond coefficients are smaller than unity. The values of α^2 for the enBt-x samples are in the range $\alpha^2 = 0.77$−0.83, indicating that around 80% of the spin population is in the copper $d_{x^2-y^2}$ orbital, suggesting a moderate covalency for the σ-bonding. A comparison of these α^2 values with those derived for $Cu(pyalen)^{2+}$ immobilized in laponite clay ($\alpha^2 = 0.82$),[42] $Cu(cyclam)^{2+}$ intercalated in hectorite clays ($\alpha^2 = 0.79$) and saponite ($\alpha^2 = 0.80$)[41] and Cu(bis-oxazoline) immobilized in laponite ($\alpha^2 = 0.79$)[40] indicates the similarity of the copper covalency of these strong ligand field copper complexes when introduced in the laminar spaces of two-dimensional inorganic matrices.

Our data also show that the in-plane σ bonding coefficient slightly decreases from $\alpha^2 = 0.88$ for Bt-x to $\alpha^2 = 0.77$−0.83 for enBt-x samples, suggesting that the in-plane σ-bonding between ethylenediamine and the copper becomes slightly more covalent when the $Cu(en)_2$ complex is introduced in the bentonite clay. Similar trends in the α^2 bonding parameters were observed when $Cu(en)_2$ complex is encapsulated in zeolite cages.[45] Additionally, α^2 changes very little from the Cu/en solution to the enBt-x samples, suggesting that no significant changes in bonding occur in the complex when is introduced into the lamellar clay. A similar tendency were observed for $Cu(pyalen)^{2+}$, where $\alpha^2 = 0.82$ is the same for the neat complex and for the copper complex immobilized in the laponite clay[42] and for Cu(bis-oxazoline) where α^2 changes from 0.76 in the neat complex to $\alpha^2 = 0.79$ when the complex is immobilized in the laponite.[40]

Now we turn our attention to the broad line, enCu-B, associated to the exchange coupled copper ions and responsible for the most intense peaks in the spectra of Figure 8. As stated before, this feature of the data was simulated in Figure 9 by considering only the axial Zeeman interaction, and the results obtained for the parameters $g_\parallel$ and $g_\perp$ are shown in Table 5. It is noticeable that the values obtained for the g-values of species enCu-A and enCu-B are similar to each other, indicating that both species, enCu-A and enCu-B, are associated with the same type of $[Cu(en)_2]^{2+}$ complex. This corroborating evidence reinforces our initial hypothesis that the only structural difference between both paramagnetic species comes essentially from the existence of a weak exchange, $J \approx A_\parallel \approx 600$ MHz (≈ 30 mK), which causes the disappearance of the hyperfine structure in the spectrum of enCu-B species.

The spectral areas calculated from double integration of the spectra are also shown in Table 5. Considering the uncertainty of the two components fitting with a large number of parameters, the calculus of each spectral area has an uncertainty that can be as high as 20−30% (this point be further discussed later). However, it is apparent that the sum of the areas calculated for the simulated partial spectra, enCu-A and enCu-B, coincides approximately with the full spectra area calculated from the high field portion of the experimental signal (2300−4500 G), which are 1.00, 1.13, and 9.87 for the samples enBt-0.1, enBt-0.5, and enBt-1.0, respectively. This means that the amount of unidentified paramagnetic centers contributing to the experimental spectrum is small, validating the hypothesis that only two species contribute to the EPR signals at the experiment temperature (5 K). It is worthy of note that the real concentrations of samples enBt-0.1 and enBt-0.5, calculated from the stoichiometry of the products, are very close to each other (0.14 and 0.19, respectively), despite their nominal concentration following the ratio 1:5.

The relative contributions of species enCu-A to the full spectra, as estimated from the parameter "Area" in Table 5, are approximately 42, 80, and 34% for samples enBt-0.1, enBt-0.5, and enBt-1.0, respectively. Obviously, these numbers are much larger than those obtained for samples Bt-x (0, 30, and 33%), indicating a more homogeneous spatial distribution of paramagnetic centers in samples enBt-x. However, the isolated copper species (Cu-A) in sample enBt-0.1 has a smaller contribution to the EPR spectrum if compared to the more concentrated sample enBt-0.5 (the area of species B follows otherwise). Obviously, the relative areas of spectra A (or B) do not increase (or decrease) monotonically as the copper concentration decreases, and this is not what one should expect for a random distribution. Therefore, a peculiar nonlinear dependence of the

dx.doi.org/10.1021/jp408658d | J. Phys. Chem. C 2013, 117, 24042−24055

magnitude of observed spin−spin exchange contribution on the concentration of copper in the samples is apparent. Such behavior is in line with that observed for aqueous Cu^{2+}/Zn^{2+} intercalates commented above.

For a deeper understanding of the presented results, some considerations must be placed. First, classical Jahn−Teller distortions, very common in six-coordinated copper complexes, are more likely to take the form of elongating the bonds to the ligands lying along the *z*-axis, forcing an increase of the interlaminar distances of the intercalate by almost 1 Å with the increase of copper concentration (recall Figure 2 and corresponding discussion). Second, in contrast to the aqueous ions samples, Bt-*x*, the affinity of the interlaminar sites for copper bis(diethylamine) complexes is much greater than for the corresponding zinc complexes. Third, the $g_{\|}$ and $A_{\|}$ parameters calculated for all enBt-*x* samples are almost independent of the concentration *x*, which seems to contradict the X-ray data that strongly suggest a decrease of interlaminar distance with the increase of zinc concentration.

From these considerations we can hypothesize that, in this kind of matrices, the interaction between paramagnetic centers is mainly favored by two different phenomena: (i) the turbostratic disorder of the clay sheets that can induce a decrease in the average intercationic distance, as determined by the lowest energy distribution of charges in individual sheets, and (ii) segregation of the paramagnetic centers from its diluted state, that is, a bidimensional statistical mixture with diamagnetic "diluents" cationic species. Segregated intercalation, typical of layered matrices, may be influencing intercalates distribution, giving rise to interstratifications of layers characterized by sequences of sheets filled with a single type of metal complex. For medium copper concentrations, such as in sample enBt-0.5, one may expect the coexistence of copper and zinc complexes in a single sheet (a similar situation such as that proposed in the model of Figure 5); however, for copper concentrations below a certain limit, it is more likely that the copper complexes become segregated to occupy individual sheets, leaving the remaining filled only with zinc complexes. This assumption may explain the fact that the contribution of the species enCu-A for the EPR spectrum of the less concentrated sample, enBt-0.1, is well below that expected for a random distribution of paramagnetic centers. The decrease in the average distance between magnetic centers caused by interlayer turbostratic disorder could be avoided by filling the space between cations with a neutral intercalant, as an amine, which by steric effect should increase the rigidity of the system. However, the segregation of copper into interstrateficated layers appears to be always effective. Such a nonlinear phenomenon is probable determined by the energy difference between the mixed bidimensional arrangement of cations with slightly different axial lengths and that of different homocationic bidimensional arrangmements.

EPR Spectra of Partially Oriented Films of $[Cu(en)_2]^{2+}$ Exchanged-Bentonite. In Figure 10 the EPR spectra obtained with the sample enBt-0.5-film, prepared by casting in thin glass plates as described in the Experimental section, are presented. For comparison, Figure 10C shows the experimental powder spectrum of Figure 8B, obtained with the original powder sample. When the magnetic field direction is parallel to the normal axis of the plates (indicated by $\theta = 0°$ in Figure 10B), the spectrum shows the typical four parallel hyperfine lines of the Cu^{2+} ion, with a strong reduction on the perpendicular components' intensity. On the contrary, when the magnetic field direction is turned to $\theta = 90°$, the parallel hyperfine lines almost disappear, and the high field part of the spectrum increases in intensity (Figure 10A). In other words, the high (low) field parts of spectra 10A (B) and C are similar in intensity and shape.

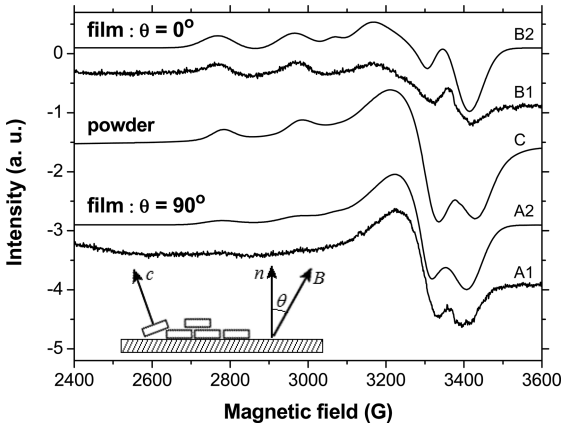

Figure 10. (Inset) A schematic representation of the bentonite platelets of sample enBt-0.5 casted on a glass plate surface. The *c*-axis is normal to the clay basal plane, and *n* is normal to the glass surface. *B* is the applied magnetic field that makes an angle θ with respect to the glass normal *n*. Noise signals are experimental EPR spectra obtained for $\theta = 0°$ (A1) and $\theta = 90°$ (B1). Noiseless traces (A2) and (B2) are the corresponding simulated spectra. For comparison the experimental powder spectrum of Figure 8B is reproduced here in C.

These features are consistent with the fact that the prepared film of bentonite is partially oriented, and the analysis of the data can be performed by a similar procedure as that used before.[2,41] Results can be interpreted by assuming that the majority of bentonite platelets are sitting with their basal planes parallel to the glass surface. If this is true, their *c*-axis should be parallel to the normal *n* of the glass surface and, also, parallel to the axial *z* axis of the paramagnetic Cu^{2+} complex. These hypotheses explain qualitatively the experimental results and are in agreement with the findings described earlier in this work.

For a more quantitative analysis we have performed a simulation of the data, in Figure 10A and B, by means of an option of the software indicated in the Experimental section, where the orientation of the paramagnetic molecules in the sample is given by the distribution:

$$P(\beta) = \exp(\lambda[3\cos(2\beta) - 1]/2) \quad (5)$$

β, in the range 0−180°, is the angle between the molecular *z* axis and the static magnetic field and the parameter λ controls the shape of the distribution. The larger the magnitude of λ, the sharper the distribution is. For positive values of λ the distribution function has maxima at $\beta = 0°$ and 180°, for negative values only at $\beta = 90°$.

Within this formalism, the best fitting was achieved by using $\lambda = 0.7$ for the data of Figure 10B ($\theta = 0°$) and $\lambda = -0.7$ for the data of Figure 10A ($\theta = 90°$). The best fitted spin Hamiltonian parameters for the species enCu-A are $g_{\|} = 2.205$, $g_{\perp} = 2.050$, $A_{\|} = 600$ MHz (200×10^{-4} cm^{-1}), $A_{\perp} = 70$ MHz (23×10^{-4} cm^{-1}), lwpp = 80 G, and for species enCu-B are $g_{\|} = 2.203$, $g_{\perp} = 2.046$, lwpp = 40 G, in close agreement with those obtained by the original powder sample (Table 5).

Temperature Dependence of the EPR Spectra of $[Cu(en)_2]^{2+}$ Exchanged-Bentonite. All of the experimental work described up to this point was accomplished about three years ago and only recently we decided to add one more experiment to study the temperature dependence of the Cu^{2+} spectra of samples enBt-*x*. This more recent experiment was

dx.doi.org/10.1021/jp408658d | J. Phys. Chem. C 2013, 117, 24042−24055

performed with aged sample enBt-0.1, and as will be described, these additional data will bring to the front important information regarding the long-range structural and magnetic ordering of the intercalated species in bentonite. During this period the sample was stored in an Eppendorf pipette, double-sealed with parafilm tape.

The first observation about this aged enBt-0.1 sample is that its EPR spectrum shows some differences with respect to the fresh sample. Both spectra are shown in Figure 11, and the spin

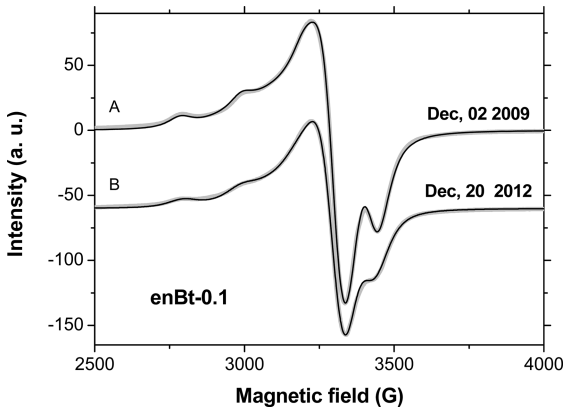

Figure 11. X-band EPR spectra of the enBt-0.1 sample measured at two occasions, separated by a time interval of three years. Fresh (A) and aged (B) samples were measured at 5 K and 4 K, respectively. Signal intensities are normalized to the Fe^{3+} resonance band.

Hamiltonian parameters obtained from the simulation are listed in Table 6. Comparison between the data in Figure 11 and Table 6 indicates that the spectra have similar g and A parameters for both components enCu-A and enCu-B; however, the main differences are related to the line broadening parameters and resulting partial spectral areas. The area of component A increased from 0.4 to 0.55, while component B decreased from 0.62 to 0.4 with aging. Also, the line broadening parameter, Hs, has assumed higher values for the aged sample, being responsible for the decrease in the resolution of the spectrum of Figure 11B. Turbostratic effects acting during the three years of sample aging may be responsible for the spatial rearrangement of the intercalated, as detected by these EPR lineshapes changes.

These results seem to indicate that there is no drastic changes in the local structure of the copper complexes influenced by aging processes, however, seem also to indicate that some rearrangements of the long-range structure of the intercalate takes place as the samples age. We have not enough experimental data to quantify this aging process, but indeed, the increase in the amount of isolated species (type A) with respect to coupled species (type B) with aging seems to indicate that such arrangements happens because the tendency to homogenize the distribution of the paramagnetic centers in the intercalate, what, for a random distribution, leads to an increase in type A with respect to type B species.

The temperature dependence of the EPR spectrum of sample enBt-0.1 was performed with the aged sample, and a few selected results are shown in Figure 12. Instead normalizing the

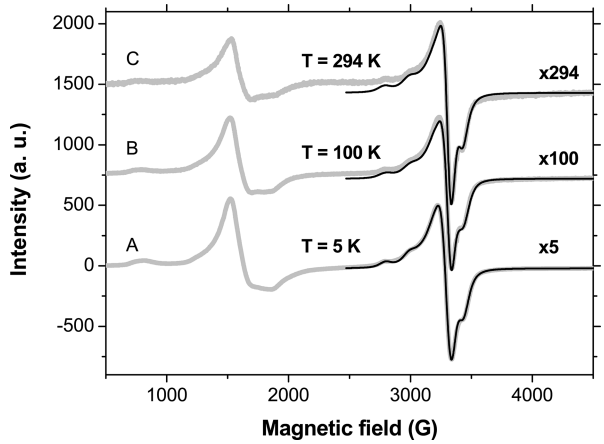

Figure 12. Typical X-band EPR spectra of the enBt-0.1 aged sample at some selected temperatures. Experimental spectra are shown in thick gray traces and corresponding fitting of the Cu^{2+} band in solid black lines. The intensity of each spectrum is normalized to the corresponding temperature.

spectra with respect to the Fe^{3+} band, as it was done before, the data in this figure were normalized to the correspondent temperature (in K). This procedure should lead to normalized spectra of same intensity, independently on the temperature, if the static magnetization follows a Curie-like behavior. In solid traces the numerical simulation of the spectra are shown, and a visible detail deserves some comments. As the temperature increases, the simulation seems to be less efficient in fitting the broad baseline, although being effective in fitting the structured line shape. This fact means that spectral features that are not visible at 4−5 K become apparent as the temperature increases. Therefore, the simple procedure of double integration of the experimental data, with the objective to calculate the joint magnetization of both species enCu-A and enCu-B, may lead to an erroneous interpretation of the physics involved in the temperature dependent magnetization behavior.

Following this remark, the experimental Cu^{2+} spectra were individually simulated at each temperature, making it possible to calculate the areas of spectra enCu-A and enCu-B, separately. With this procedure the plot of the areas, as a function of temperature, can be assigned without much interference from baseline artifacts, and the results can be appreciated in Figure 13. In this figure the inverse of the individual areas of species A and B are plotted, as well as the inverse of their sum. It is evident that the plotted data can be characterized by the linear behavior predicted by the Curie law. The ratio

Table 6. Spin Hamiltonian Parameters for the Simulated Spectra of Figure 11[a]

species	sample	area	$g_\perp$	$g_\parallel$	$A_\perp$ (MHz)	$A_\parallel$ (MHz)	lwpp (G)	$Hs_\perp$ (MHz)	$Hs_\parallel$ (MHz)
enCu-A	fresh	0.40	2.039	2.190	92	615	44	167	101
	aged	0.62	2.044	2.195	119	582	55	195	171
enCu-B	fresh	0.55	2.053	2.206			46	137	1036
	aged	0.40	2.051	2.190			0	279	897

[a]The nomenclature is the same as that of Table 4.

dx.doi.org/10.1021/jp408658d | J. Phys. Chem. C 2013, 117, 24042−24055

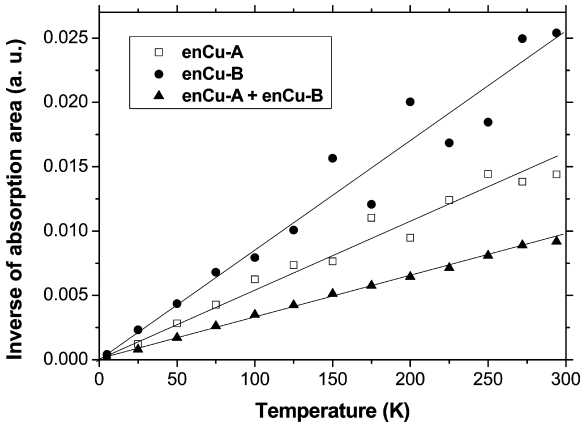

Figure 13. Temperature dependence of the absorption area for the two Cu^{2+} components: isolated species, enCu-A (open squares) and magnetic coupled species, enCu-B (black circles). The sum of both areas, representing the full spectrum area, is in black triangles.

area(enCu-A)/area(enCu-B) varies randomly from 1.1 to 2.1, in the entire temperature range, with the average value of 1.6 coinciding with the ratio 0.62/0.40 = 1.55 obtained at 4 K (Table 6). Such considerable fluctuation of the data points is a result of about 20−30% of uncertainty in the determination of each individual area. As can be noted, the large displacement of the data points relative to the straight lines are more pronounced in the individual contributions than in their joint results. In other words, all three data sets seem to follow a straight line crossing the origin, but the data corresponding to the joint contributions of species A and B (black triangles) are less noisy. In part, this is a visual effect caused by the inverse vertical scale, but it is also caused by some degree of cross-correlation between the fitting parameters of species A and B, leading to uncertainties of the partial fits. Indeed, some correlation can be seen in the plots of A and B data, that is, if a given data point of A is above the straight line, the corresponding data B is below the straight line (and otherwise), making the sum of A and B almost insensitive to partial fitting uncertainties.

From these data, it can be concluded that the magnetization associated to the two paramagnetic species enCu-A and enCu-B in sample enBt-01 follows a Curie-like behavior, indicating that they can be, both, associated to isolated paramagnetic centers. This affirmation means that the exchange interaction acting in species enCu-B are, indeed, very weak and incapable to produce long-range magnetization effects, although strong enough to collapse (or broaden) the hyperfine interaction.

This conclusion is consistent with the values of the geometric parameter G, which is a measure of the exchange interaction between copper centers and is calculated using the equation $G = (g_{\|} - 2.0023)/(g_{\perp} - 2.0023)$ for axial spectra.[70] If $G > 4$ the exchange interaction is negligible. In the case of samples enBt-x, with x = 0.1, 0.5, and 1.0, this parameter results, respectively, G = 5.1, 3.6, and 4.9 for species enCu-A and G = 4.0, 4.8, and 3.2 for enCu-B.

CONCLUSIONS

The EPR behavior of two-dimensional networks of Cu^{2+} ions, built by exchanging Na-bentonite with Cu^{2+} aqueous or with bis(ethylenediamine) complex, $[Cu(C_2H_4(NH_2))_2]^{2+}$, at different concentrations of the paramagnetic center is studied. Dilution of the magnetically active species is performed by saturating the intrinsic charge of the clay, cec, by the cointercalation of analogous diamagnetic zinc species: aqueous Zn^{2+} or complexed $[Zn(C_2H_4(NH_2))_2]^{2+}$ ions. Ion exchange experiments indicate that the relative affinity of both aqueous ions for bentonite is similar. In contrast, the affinity of the interlaminar sites for copper−bis(ethylenediamine) complexes is much greater than for the corresponding zinc complexes.

EPR results on Cu^{2+}/Zn^{2+} exchanged bentonite samples support the view that the paramagnetic copper centers are not uniformly distributed in the interlaminar space of the clay, at any concentration, suggesting a tendency to clustering that increases as the concentration decreases. The cointercalation of copper and zinc ions in the presence of ethylenedimine leads, independently of the reaction procedure, or the excess of amine, to the insertion of copper-bis(ethylenediamine) complexes, in which the respective fifth and sixth coordination sites are saturated by oxygen atoms from the clay surface. Besides, prepared products contain a great excess of amine located in the interlayer space between metallic centers, which favors immobilization, dilution, and homogeneity of the spatial distribution of paramagnetic centers.

For all samples, the EPR spectra were deconvoluted in two components, corresponding to the spin−spin exchanged species (broad spectrum) and isolated ones (hyperfine structured spectrum). The origin of the broad component was explained by the existence of weak exchange interactions (of the order of 20−30 mK) that are capable to smear the hyperfine interactions. Temperature dependence of the EPR spectra of the intercalated Cu-bis(ethylenediamine) complexes shows that the static susceptibility follows the Curie law for both species, indicating that exchange interactions are small and not capable to produce long-range magnetic ordering.

All measurements are in agreement with the proposed model in which the axial axis of the intercalated Cu/bis(ethylenediamine) complexes is coincident with the bentonite c-axis. This fact was confirmed by the angular dependency of the EPR spectra in partially oriented films casted in glass plates.

X-ray diffraction measurements indicated that the interlaminar distance in the bentonite decreases with the increase of Zn concentration in the Cu/en composites. Additionally, the spin Hamiltonian parameters $g_{\|}$ and $A_{\|}$ determined by EPR measurements are insensitive to the laminar distance variations, indicating segregation of paramagnetic ions by interstratifications of layers.

In essence, this work analyzes the feasibility of diluting cationic paramagnetic species with diamagnetic cations in the two-dimensional interlaminar space defined by negatively charged sheets, like those in layered natural clays. In this kind of matrices the interaction between paramagnetic centers is mainly favored by two different phenomena: (i) the turbostratic disorder of the clay sheets and (ii) segregation of the magnetic centers from its diluted state leading to interstratifications of layers. The experimental approach used in this work strongly influences the interactions between paramagnetic centers. First, the effects of interlayer turbostratic disorder are reduced by filling the free space between the cations with a neutral intercalant, which increases the rigidity of the system. Second, segregation characterized by interstratifications is a mandatory effect that depends on the compatibility of both, magnetic centers and diluents species, with the matrix. The more similar the nature and properties of both species, the lower the molar ratio will be at which segregation in different sheets will occurs. Cu^{2+} and Zn^{2+} ions are very similar; however, the Jahn−Teller effect has an important influence that, in this case, will cause the observed segregation.

dx.doi.org/10.1021/jp408658d | J. Phys. Chem. C 2013, 117, 24042−24055

AUTHOR INFORMATION

Corresponding Author

*E-mail: donoso@ifsc.usp.br.

Notes

The authors declare no competing financial interest.

ACKNOWLEDGMENTS

Research partially financed by FONDECYT (Contracts 113112, 111029), Basal Financing Program CONICYT, FB0807 (CEDENNA), Millennium Science Nucleus P06-022-F, and CeRTEV, Center for Research, Technology and Education in Vitreous Materials, Fapesp 2013/07793-6. Partial support of CNPq is gratefully acknowledged. The authors wish to acknowledge Karie Friedman for helpful comments.

REFERENCES

(1) Pinnavaia, T. J. Intercalated Clay Catalysts. *Science* **1983**, *220*, 365−371.

(2) Giannelis, E. Highly Organized Molecular Assemblies of Porphyrin Guest Molecules in Mica-Type Silicates: Influence of Guest-Host Interaction on Molecular Organization. *Chem. Mater.* **1990**, *2*, 627−629.

(3) Mehrotra, V.; Giannelis, E. P. Intercalation of Ethylenediamine Functionalized Buckminsterfullerene in Mica-Type Silicates. *Chem. Mater.* **1992**, *4*, 20−22.

(4) Lezhnina, M.; Benavente, E.; Bentlage, M.; Echeverria, Y.; Klumpp, E.; Kynast, U. Luminescent Hybrid Materials Based on a Clay Mineral. *Chem. Mater.* **2007**, *19*, 1098−1102.

(5) Celedon, S.; Quiroz, C.; Gonzalez, G.; Sotomayor, C. M.; Benavente, E. Lanthanides-Clay Nanocomposites: Syntesis, Characterization and Optical Properties. *Mater. Res. Bull.* **2009**, *44*, 1191−1194.

(6) Khaorapapong, N. *In situ* Complexation of Thiourea in the Interlayer Space of Copper(II) - Monmorillonite. *Appl. Clay Sci.* **2010**, *50*, 414−417.

(7) Malla, P. B.; Ravindranathan, P.; Komarneni, S.; Roy, R. Intercalation of copper metal clusters in montmorillonite. *Nature* **1991**, *351*, 555−557.

(8) Carriazo, J.; Guélou, E.; Barrault, J.; Tatibouet, J. M.; Molina, R.; Moreno, S. Synthesis of Pillared Clays Containing Al, Al-Fe or Al-Ce-Fe from a Bentonite: Characterization and Catalytic Activity. *Catal. Today* **2005**, *107−108*, 126−132.

(9) Chmielarz, L.; Piwowarska, Z.; Kustrowski, P.; Gil, B.; Adamski, A.; Dudek, B.; Michalik, M. Porous Clay Heterostructures (PCHs) Intercalated with Silica-Titania Pillars and Modified with Transition Metals as Catalysts for the DeNOx Process. *Appl. Catal., B* **2009**, *91*, 449−459.

(10) Gonzalez Bahamon, L. F.; Hoyos, D. F.; Benitez, N.; Pulgarin, C. New Fe-Immobilized Natural Bentonite Plate Used as Photo-Fenton Catalyst for Organic Pollutant Degradation. *Chemosphere* **2011**, *82*, 1185−1189.

(11) Pavlidou, S.; Papaspyrides, C. D. A Review on Polymer-Layered Silicate Nanocomposites. *Prog. Polym. Sci.* **2008**, *33*, 1119−1198.

(12) Moreno, M.; Santa Ana, M. A.; Gonzalez, G.; Benavente, E. Poly(acrylonitrile)- Montomorillonite Nanocomposites. Effects of the Intercalation of the Filler on the Conductivity of Composite Polymer Electrolytes. *Electrochim. Acta* **2010**, *55*, 1323−1327.

(13) Bitinis, N.; Hernandez, M.; Verdejo, R.; Kenny, J. M.; Lopez Manchado, M. A. Recent Advances in Clay/Polymer Nanocomposites. *Adv. Mater.* **2011**, *23*, 5229−5236.

(14) Sanchez, A.; Echeverria, Y.; Sotomayor Torres, C. M.; González, G.; Benavente, E. Intercalation of Europium (III) Species into Bentonita. *Mater. Res. Bull.* **2006**, *41*, 1185−1191.

(15) Safa Özcan, A.; Gök, Ö.; Özcan, A. Adsorption of Lead(II) Ions onto 8-Hydroxy Quinoline - Immobilized Bentonite. *J. Hazard. Mater.* **2009**, *161*, 499−509.

(16) Abou-El-Sherbini, K. S.; Hassanien, M. M. Study of Organically Modified Montmorillonite Clay for the Removal of Copper(II). *J. Hazard. Mater.* **2010**, *184*, 654−661.

(17) Veli, S.; Alyüz, B. Adsorption of Copper and Zinc from Aqueous Solutions by using Natural Clay. *J. Hazard. Mater.* **2007**, *149*, 226−233.

(18) Yagubov, A. I.; Binnatova, L. A.; Muradova, N. M.; Nuriev, A. N. Wastewater Purification to Remove Dyes with Monocation-Substituted Forms of Bentonite and Flocculants-Coagulants. *Russ. J. Appl. Chem.* **2010**, *83*, 420−423.

(19) Alandis, N. M.; Aldayel, O. A.; Mekhemer, W. K.; Hefne, J. A.; Jokhab, H. A. Thermodynamic and Kinetic Studies for the Adsorption of Fe(III) and Ni(II) Ions From Aqueous Solution using Natural Bentonite. *J. Dispersion Sci. Technol.* **2010**, *31*, 1526−1534.

(20) Chen, L.; Yu, S.; Huang, L.; Wang, G. Impact of Environmental Conditions on the Removal of Ni(II) from Aqueous Solution to Bentonite/Iron Oxide Magnetic Composites. *J. Radioanal. Nucl. Chem.* **2012**, *292*, 1181−1191.

(21) Zhu, L.; Ren, X.; Yu, S. Use of Cetyltrimethyl ammonium Bromide-Bentonite to Remove Organic Contaminants of Varying Polar Character from Water. *Environ. Sci. Technol.* **1998**, *32*, 3374−3378.

(22) Banat, F. A.; Al-Bashir, B.; Al-Aseheh, S.; Hayajneh, O. Adsorption of Phenol by Bentonite. *Environ. Pollut.* **2000**, *107*, 391−398.

(23) Pateiro-Moure, M.; Nóvoa-Muñoz, J. C.; Arias-Estévez, M.; López-Periago, E.; Martínez-Carballo, E.; Simal-Gándara, J. Quaternary Herbicides Retention by the Amendment of Acid Soils with a Bentonite-Based Waste from Wineries. *J. Hazard. Mater.* **2009**, *164*, 769−775.

(24) Rahardjo, A. K.; Susanto, M. J. J.; Kurniawan, A.; Indraswati, N.; Ismadji, S. Modified Ponorogo Bentonite for the Removal of Ampicillin from Wastewater. *J. Hazard. Mater.* **2011**, *190*, 1001−1008.

(25) Díaz-Navas, M. C.; Olguín, M. T.; Solache-Ríos, M. Adsorption of Phenol onto Surfactants Modified Bentonite. *J. Incl. Phenom. Macrocycl. Chem.* **2012**, *74*, 67−75.

(26) Couture, R. A. Steam Rapidly Reduces the Swelling Capacity of Bentonite. *Nature* **1985**, *318*, 50−52.

(27) Villar, M. V. Water Retention of Two Natural Compacted Bentonites. *Clays Clay Miner.* **2007**, *55*, 311−322.

(28) Jedináková-Krizová, V.; Zeman, J.; Vinsová, H.; Hanslík, E. Bentonite Stability, Speciation and Migration Behaviour of some Critical Radionuclides. *J. Radioanal. Nucl. Chem.* **2010**, *286*, 719−727.

(29) Ghiaci, M.; Sadeghi, Z.; Sedaghat, M. E.; Karimi-Maleh, H.; Safaei-Ghomi, J.; Gil, A. Preparation of Pd (0) and Pd (II) Nanotubes and Nanoparticles on Modified Bentonite and their Catalytic Activity in Oxidation of Ethyl Benzene to Acetophenone. *Appl. Catal., A* **2010**, *381*, 121−131.

(30) Bendedouche, C. K.; Benhaoua, H. Copper Exchanged Bentonite: a Reusable Catalysis for the Formation of Alkoxycarbonyl Nitrile Ylides under Microwave Irradiation. *J. Chem. Res.* **2012**, *3*, 149−151 ed.

(31) Pilbrow, J. R. *Transition Ion Electron Paramagnetic Resonance*; Clarendon Press: Oxford, U.K., 1990.

(32) Brown, D. R.; Kevan, L. Aqueous Coordination and Location of Exchangeable Cu^{2+} Cations in Montmorillonite Clay Studied by Electron Spin Resonance and Electron Spin-Echo Modulation. *J. Am. Chem. Soc.* **1988**, *110*, 2743−2748.

(33) Annabi-Bergaya, F.; Estrade-Szwarckopf, H.; Van Damme, H. Dehydration of Cu-Hectorite: Water Isotherm, XRD, and EPR Studies. *J. Phys. Chem.* **1996**, *100*, 4120−4126.

(34) Hyun, S. P.; Cho, Y. H.; Kim, S. J.; Hahn, P. S. Cu(II) Sorption Mechanism on Montmorillonite: An Electron Paramagnetic Resonance Study. *J. Colloid Interface Sci.* **2004**, *222*, 254−261.

(35) Strawn, D. G.; Palmer, N. E.; Furnare, L. J.; Goodell, C.; Amonette, J. F.; Kukkadapu, R. K. Copper Sorption Mechanisms on Smectites. *Clays Clay Miner.* **2004**, *52*, 321−333.

(36) Carriazo, J.; Molina, R.; Moreno, S. A Study on Al and Al−Ce−Fe Pillaring Species and their Catalytic Potential as they are Supported on a Bentonite. *Appl. Catal., A* **2008**, *334*, 168−172.
(37) De Santana, H.; Paesano, A.; da Costa, A. C. S.; di Mauro, E.; de Souza, I. G.; Ivashita, F. F.; de Souza, C. M. D.; Zaia, C. T. B. V.; Zaia, D. A. M. Cysteine, Thiourea and Thiocyanate Interactions with Clays: FT-IR, Mössbauer and EPR Spectroscopy and X-Ray Diffractometry Studies. *Amino Acids* **2010**, *38*, 1089−1099.
(38) Velghe, F.; Schoonheydt, R. A.; Uytterhoeven, J. B.; Peigneur, P.; Lunsford, J. H. Spectroscopic Characterization and Thermal Stability of Copper(II) Ethylenediamine Complexes on Solid Surfaces. 2. Montmorillonite. *J. Phys. Chem.* **1977**, *81*, 1187−1194.
(39) Goodman, B. A.; Green, H. L.; McPhail, D. B. An Electron Paramagnetic Resonance Study of the Adsorption of Copper Complexes on Montmorillonite and Imogolite. *Geochim. Cosmochim. Acta* **1984**, *48*, 2143−2150.
(40) Alonso, P. J.; Fraile, M.; García, J.; García, J. I.; Martínez, J. I.; Mayoral, J. A.; Sanchez, M. C. Spectroscopic Study of the Structure of Bis(oxazoline) Copper Complexes in Solution and Immobilized on Laponite Clay. Influence of the Structure on the Catalytic Performance. *Langmuir* **2000**, *16*, 5607−5612.
(41) So, H.; Jung, H.; Choy, J.-H.; Linn Belford, R. Electron Paramagnetic Resonance Study of Partially Oriented Clay Platelets Intercalated with Copper(II) 1,4,8,11 Tetraazacyclotetradecane. *J. Phys. Chem. B* **2005**, *109*, 3324−3329.
(42) Dias, P. M.; Kinouti, L.; Constantino, V. R. L.; Ferreira, A. M. D. C.; Gonçalves, M. B.; do Nascimento, R. R.; Petrilli, H. M.; Caldas, M.; Frem, R. C. G. Spectroscopic Characterization of Schiff Base-Copper Complexes Immobilized in Smectite Clays. *Quim. Nova* **2010**, *33*, 2135−2142.
(43) Ray, R. K.; Kauffman, G. B. EPR Spectra and Covalency of Bis (amidinourea/O-alkyl-1-amidinourea) copper(II) Complexes. Part II. Properties of the CuN_4^{2-} Chromophore. *Inorg. Chim. Acta* **1990**, *173*, 207−214.
(44) Bergaya, F.; Vayer, M. CEC of Clays: Measurement by Adsorption of a Copper Ethylenediamine Complex. *Appl. Clay Sci.* **1997**, *12*, 275−280.
(45) Ganesan, R.; Viswanathan, B. Physicochemical and Catalytic Properties of Copper Ethylenediamine Complex Encapsulated in Various Zeolites. *J. Phys. Chem. B* **2004**, *108*, 7102−7114.
(46) Peigneur, P.; Lunsford, J. H.; De Wilde, W.; Schoonheydt, R. A. Spectroscopic Characterization and Thermal Stability of Copper(II) Ethylenediamine Complexes on Solid Surfaces. 1. Synthetic Faujasites Types X and Y. *J. Phys. Chem.* **1977**, *81*, 1179−1187.
(47) Lewis, W. B.; Alei, M.; Morgan, L. O. Magnetic-Resonance Studies on Copper(lI) Complex Ions in Solution. II. Oxygen-l 7 NMR and Copper(lI) EPR in Aqueous Solutions of $Cu(en)(H_2O)_4$ and $Cu(en)_2(H_2O)_2$. *J. Chem. Phys.* **1966**, *45*, 4003−4013.
(48) Stoll, S.; Schweiger, A. EasySpin, a Comprehensive Software Package for Spectral Simulation and Analysis in EPR. *J. Magn. Reson.* **2006**, *178*, 42−55.
(49) Bacsik, Z.; Atluri, R.; Garcia-Bennett, A. E.; Hedin, N. Temperature Induced Uptake of CO_2 and Formation of Carbamates in Mesocages Silica Modified with n-Propylamines. *Langmuir* **2010**, *26*, 10013−10024.
(50) Zhou, Q.; Frost, R. L.; He, H.; Xi, Y. Changes in the Surfaces of Adsorbed *p*-Nitrophenol on Methyl trioctadecylammonium Bromide Organoclay - an XRD, TG, and Infrared Spectroscopic Study. *J. Colloid Interface Sci.* **2007**, *314*, 405−414.
(51) Bahranowski, K.; Dula, R.; Labanowska, M.; Serwicka, E. M. ESR Study of Cu Centers Supported on AI-, Ti-, and Zr-Pillared Montmorillonite Clays. *Appl. Spectrosc.* **1996**, *50*, 1439−1445.
(52) Donoso, J. P.; Tambelli, C. E.; Magon, C. J.; Mattos, R. I.; Silva, I. D. A.; Souza, J. E.; Moreno, M.; Benavente, E.; Gonzalez, G. Nuclear Magnetic Resonance Study of Hydrated Bentonite. *Mol. Cryst. Liq. Cryst.* **2010**, *521*, 93−103.
(53) Griscom, D. L. Electron Spin Resonance in Glasses. *J. Non-Cryst. Solids* **1980**, *40*, 211−272.
(54) Singh, R. K.; Srinivasan, A. EPR and Magnetic Properties of $MgO-CaO-SiO_2-P_2O_5-CaF_2-Fe_2O_3$ Glass-Ceramics. *J. Magn. Magn. Mater.* **2009**, *321*, 2749−2752.
(55) Muralidhara, R. S.; Kesavulu, C. R.; Rao, J. L.; Anavekar, R. V.; Chakradhar, R. P. S. EPR and Optical Absorption Studies of Fe^{3+} ions in Sodium Borophosphate Glasses. *J. Phys. Chem. Solids* **2010**, *71*, 1651−1655.
(56) Castner, T.; Newell, G. S., Jr.; Holton, W. C.; Slichter, C. P. Note on the Paramagnetic Resonance of Iron in Glasses. *J. Chem. Phys.* **1960**, *32*, 668−673.
(57) Schneider, H.; Rager, H. Iron Incorporation in Mullite. *Ceram. Int.* **1986**, *12*, 117−125.
(58) Anderson, P. W. A Mathematical Model for the Narrowing of Spectral Lines by Exchange or Motion. *J. Phys. Soc. Jpn.* **1954**, *9*, 316−339.
(59) Farach, H. A.; Strother, E. F.; Poole, C. P. Solution to Anderson Exchange Narrowing Model for *I* Greater than 1/2. *J. Phys. Chem. Solids* **1970**, *31*, 1491−1510.
(60) Calvo, R.; Isern, H.; Mesa, M. A. EPR Study of $Cu(L\text{-}Ile)_2$, a Copper Amino acid Salt. *Chem. Phys.* **1985**, *100*, 89−99.
(61) Hyun, S. P.; Cho, Y. H.; Hahn, P. S. An Electron Paramagnetic Resonance Study of Cu(II) Sorbed on Kaolinite. *Appl. Clay Sci.* **2005**, *30*, 69−78.
(62) Yu, J. S.; Ryoo, J. W.; Kim, S. J.; Hong, S. B.; Kevan, L. Cupric Ion Species in Cu(II)-Exchanged K-Offretite Gallosilicate Determined by Electron Spin Resonance and Electron Spin Echo Modulation Spectroscopies. *J. Phys. Chem.* **1996**, *100*, 12624−12630.
(63) Kim, J. Y.; Yu, J.-S.; Kevan, L. Location of Cupric Ion and its Adsorbate Interactions in Cu(II) Exchanged Mesoporous AlMCM-41 Determined by Electron Spin Resonance and Electron Spin Echo Modulation. *Mol. Phys.* **1998**, *95*, 989−997.
(64) Carl, P. J.; Larsen, S. C. EPR Study of Copper-Exchanged Zeolites: Effects of Correlated *g*- and *A*-Strain, Si/Al Ratio, and Parent Zeolite. *J. Phys. Chem. B* **2000**, *104*, 6568−6575.
(65) Peisach, J.; Blumberg, W. E. Structural Implications Derived from the Analysis of Electron Paramagnetic Resonance Spectra of Natural and Artificial Copper Proteins. *Arch. Biochem. Biophys.* **1974**, *165*, 691−708.
(66) Sakaguchi, U.; Addison, A. W. Spectroscopic and Redox Studies of Some Copper(II) Complexes with Biomimetic Donor Atoms: Implications for Protein Copper Centres. *J. Chem. Soc., Dalton Trans.* **1979**, *4*, 600−608 ed.
(67) Kivelson, D.; Neiman, R. ESR Studies on the Bonding of Copper Complexes. *J. Chem. Phys.* **1961**, *35*, 149−155.
(68) Gersmann, H. R.; Swalen, J. D. Electron Paramagnetic Resonance of Copper Complexes. *J. Chem. Phys.* **1962**, *36*, 3221−3233.
(69) Boobalan, S.; Rao, P. S. Structural Elucidation of Cu(II) Ion Doped in Hexaaquozinc diaquobis (malonato) Zincate Host by EPR Spectroscopy. *J. Phys. Chem. Solids* **2010**, *71*, 1527−1533.
(70) Singh, B. K.; Bhojak, N.; Mishra, P.; Garg, B. S. Copper(II) Complexes with Bioactive Carboxyamide: Synthesis, Characterization and Biological activity. *Spectrochim. Acta A* **2008**, *70*, 758−765.